2005 유체기계 연구개발 발표회 논문집, pp. 3~13
창원대학교 국제교류센터 및 정보전산원 2005. 12. 1~2

Unsteady Flow Due to Rotor-Stator Interaction in Diffuser Pumps

By

Hiroshi TSUKAMOTO

Department of Biological Functions and Engineering, Graduate School of
Life Science and Systems Engineering, Kyushu Institute of Technology
2-4, HIbikino, Wakamatsu, Kitakyushu, 808-0196 Japan

Introduction

In diffuser pumps, the centrifugal impeller interferes with the diffuser vanes and produces pressure fluctuations downstream of the impeller. These pressure fluctuations not only generate noise and vibration that cause unacceptable levels of stress and reduce component life due to fatigue, but also introduce unfavorable characteristics of pump performance even at or near the design point. Such unsteady phenomena in diffuser pumps become more complicated at off-design operating conditions. This paper presents the experimental and numerical data on rotor-stator interaction phenomena in diffuser pump by the present authors.

Unstable Characteristics of Diffuser Pump

The static characteristics of diffuser pumps with a positive slope in its steady characteristic curve were classified based on experimental and numerical study [(1)]. Experimental study was made to measure unsteady flow profiles at the impeller inlet and exit, as well as the pressure on the casing wall of vaned diffuser passage for understanding the instability of the pump under steady operation [(2)]. Two diffuser pumps' data will be shown in this paper. The principal specifications of the pump are summarized in Table 1. Test pump A is a centrifugal pump with a closed impeller illustrated in Figure 1(a), and corresponds to one stage of a multi-stage centrifugal pump. Test pump B is a mixed flow pump with an open impeller, specific speed Ns = 624 [m^3/min, m, min^{-1}], as illustrated schematically in Fig. 1(b). Unsteady flow was measured on the measurement stations at upstream and downstream of the test pump B impeller, *CSI* and *CSII*, by traversing a fast response five-hole pitot-tube. Figures 1(a-2) and 1(b-2) illustrate the unsteady pressure measurement stations on the shroud casing of the diffuser in the test pumps. The measurement stations were arranged on the intersection of six radial and five stream-wise grid lines in a blade-to-blade diffuser passage for test pump A. The unsteady pressure measurement stations on the casing wall of a guide vane passage ware arranged on the intersection of four radial and five stream-wise grid lines in a blade-to-blade passage for pump B.

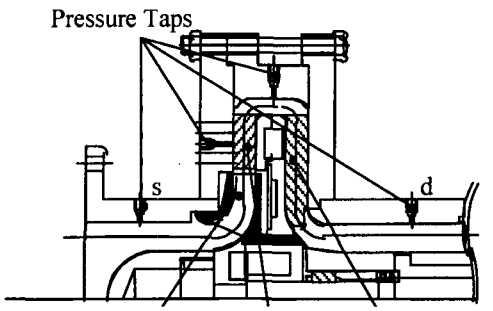

(a-1) **Cross-sectional view of test pump A**

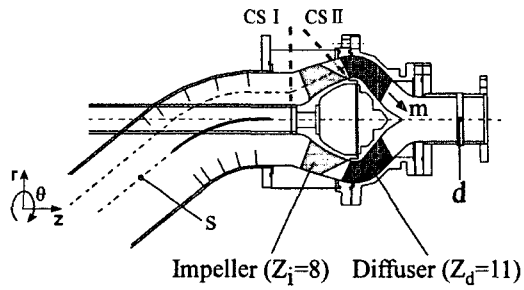

(b-1) **Cross-sectional view of test pump B**

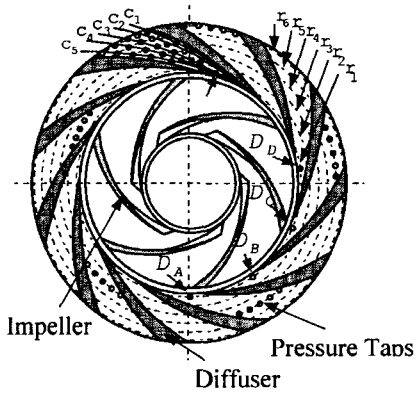

(a-2) **impeller and diffuser**

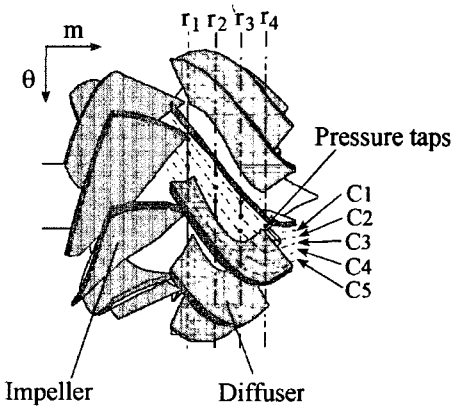

(b-2) **Impeller and diffuser**

Fig. 1 Schematic configurations of test diffuser pump

Table 1 Specifications of test pumps

	Pump A	Pump B
Suction diameter D_s	200 mm	220 mm
Discharge diameter D_d	200 mm	102.81 mm
Impeller:		
R_2	165 mm	129.98 mm
Z_i	6	8
Diffuser:		
R_3	170 mm	150.98 mm
R_4	240 mm	93.5 mm
Z_d	11	11
Return Channel:		
R_5	240 mm	None
R_6	120.5 mm	None
Z_r	11	None
Rating:		
Q_r	4.4 m^3/min	10.56 m^3/min
H_r	33.7 m	19.75 m
N_r	1500 min^{-1}	1800 min^{-1}
Ns (m^3/min,m,min^{-1})	232	624

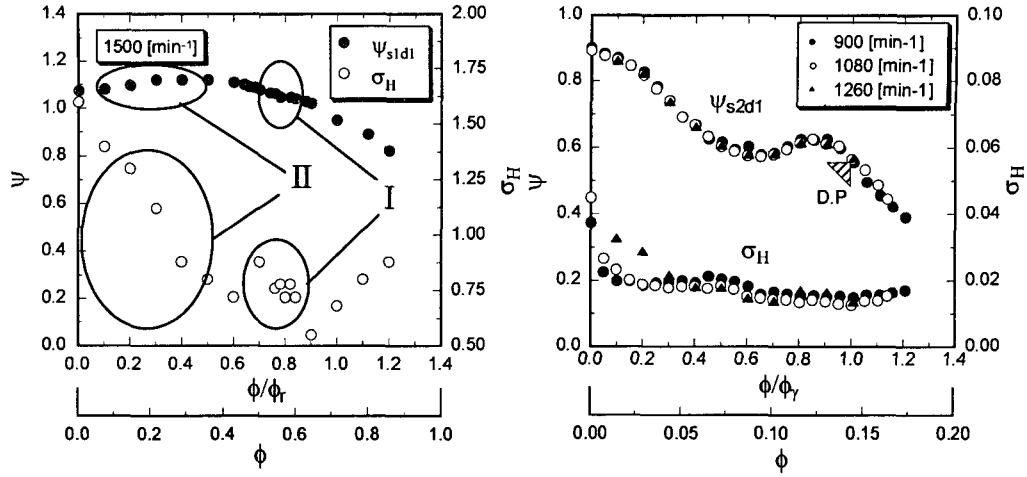

(a) Pump A **(b) Pump B**

Fig. 2 Test pump characteristic curves and standard deviation of total pressure rise

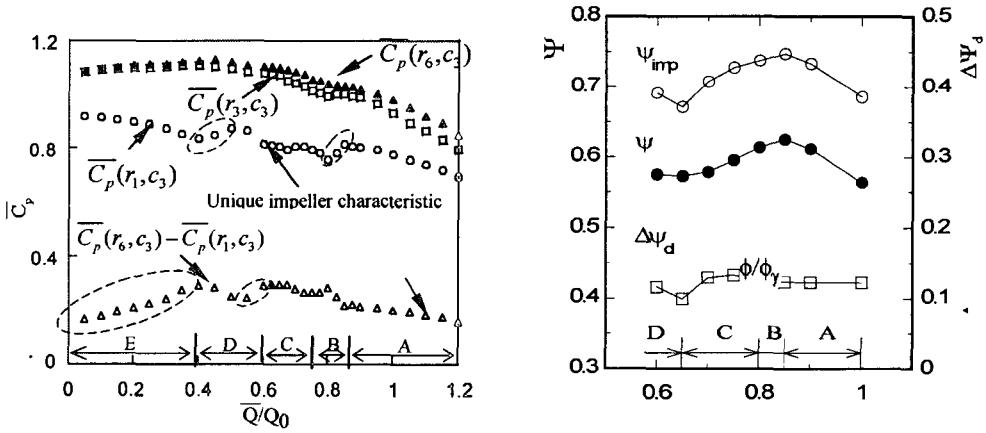

(a) Test pump A ***(b) Test pump B***

Fig. 3 Impeller characteristic and hydraulic loss in the diffuser vane

Figure 2 shows the measured total pressure rise coefficient ψ and its standard deviation, σ_ψ of two test pumps. The performance curve of Pump A shows that there exist an evident positive slope below the 50 percent of the rated flow rate designated by *II*, and a slightly positive slope in a very small range at approximately 80 percent of the rated flow rate designated by *I*.

There exists distinct strong positive slope on the characteristics from 65 to 85 percent of the rated flow rate for Pump B, as can be seen in Fig. 2(b). As is well known, the diffuser pump becomes unstable when operating in these ranges with positive slope of

characteristic curve. Whereas there exist marked increase in σ_ψ in these two ranges designated by *I* ($\phi/\phi_r \cong 0.8$) and *II* ($\phi/\phi_r < 0.5$) for Pump A, there are not remarkable variation in σ_ψ although the σ_ψ increases with decreasing flow rate. Therefore an unstable characteristic cannot always be related to a marked change in σ_ψ.

Unsteady flow was measured at upstream and downstream of impeller, as well as on the casing wall of diffuser passage by using a fast response five-hole pitot-tube and/or semi-conductor type pressure transducers. As a result of the unsteady flow measurements, the positive slope of steady characteristic was found to be caused by flow separation, inlet backflow, and pre-rotation. The pressure fluctuations were analyzed using the ensemble averaging technique as well as the statistical and chaotic time series analysis.

Figure 3(a) presents the time-averaged pressure coefficient $\bar{C}_p$ on the representative pressure taps (r_1,c_3) at the inlet, (r_3,c_3) at the mid, and (r_6,c_3) at the outlet of the diffuser passage for Pump A. This figure shows also the $\{ \bar{C}_p(r_6,c_3) - \bar{C}_p(r_1,c_3)\}$ which reflects the diffuser performances. At $\phi/\phi_r \cong 0.8$ and $0.4 < \phi/\phi_r < 0.6$ the slope of $\bar{C}_p(r_1,c_3)$ is positive which shows the unique impeller performance. On the other hand, there exists positive slope of the unique diffuser performance at $\phi/\phi_r < 0.4$ and $0.5 < \phi/\phi_r < 0.7$. The entire operating range can be classified into five ranges from A to E as shown in Fig. 6(a), based on the positive slope of these characteristic curves and referring to the numerical calculated flow fields [2].

(a) Range A at $0.85 < \phi/\phi_r < 1.20$, where the pump is stable.

(b) Range B at $0.75 < \phi/\phi_r < 0.85$, where the pump is unstable because of the separating flow and stall in impeller.

(c) Range C at $0.60 < \phi/\phi_r < 0.75$, where the pump is stable.

(d) Range D at $0.40 < \phi/\phi_r < 0.60$, where the pump is unstable due to the separating flow and stall in both impeller and diffuser, which are verified in the numerical calculations.

(e) Range E at $\phi/\phi_r \lesssim$ 040, where the pump is unstable because of the separating flow and stall mainly in the diffuser.

Figure 3(b) shows the impeller characteristic and the hydraulic loss in the guide vane for test pump B. The ψ_{imp} is defined as the normalized difference of the total pressure between impeller downstream, CS_{II}, and pressure tap (s), and represents impeller characteristic. The $\Delta\psi_d$, normalized total pressure difference between CS_{II} and (d) expresses the hydraulic loss in the guide vane passage. As shown in this figure, there exists positive slope of the impeller characteristic from 65 to 85 percent of the rated

flow rate, while the hydraulic loss in the guide vane is almost constant, which indicates that a positive slope in the pump characteristic curve may be caused by impeller performance. According to the fast-response five-hole pitot-tube measurements[2], the back flow can be observed near impeller tip at inlet for $0.65 < \phi/\phi_r < 0.70$, in which there is a strong pre-rotation with big tangential velocity that reduces the impeller's Euler head and thus seems to be responsible for reduction in the total head. The numerical results of unsteady flow at a partial discharge range have supported the experimental results on unsteady phenomena at off-design condition [1][3].

Hydrodynamic Radial Forces

Big hydrodynamic forces may be caused by the pressure fluctuations due to rotor-stator interaction. Table 2 lists the standard deviation of the unsteady fluid forces K_x[4][5]. As can be seen in Table 2, the unsteady fluid forces for Z_d = 0, 2, 3 and 6 are much smaller than for Z_d = 5 and 7. The results will be presented only for 3 representative cases, Z_d = 0, 5 and 6 among the cases of Z_d = 0, 2, 3, 5, 6, and 7, in this paper. The impeller for Z_d =2 and 3 also caused smaller forces by the same mechanism as the case of Z_d = 6. And the case of Z_d =7 caused larger forces by the mechanism similar to the case of Z_d = 5.

Table 2 Standard Deviations of K_x for various diffuser vanes' number

Diffuser Blade No.	0	2	3	5	6	7
Standard Deviation	0.0044	0.0059	0.0062	0.035	0.0058	0.020

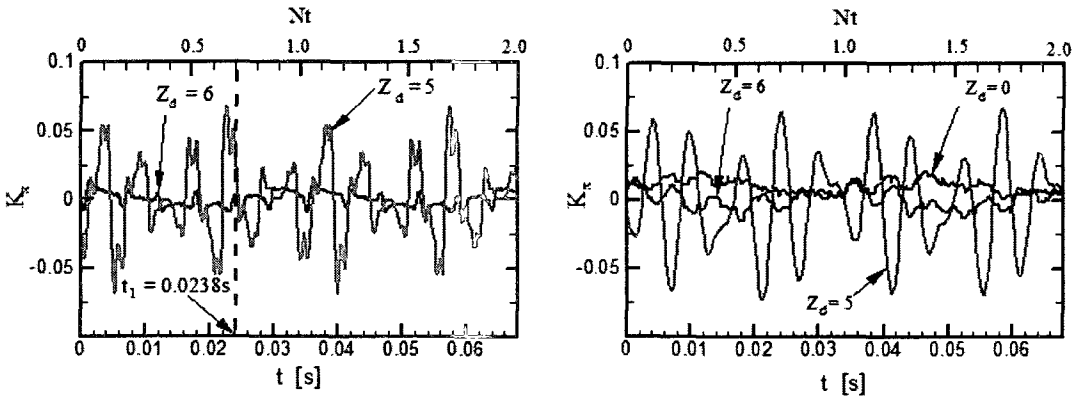

(a) Measured **(b) CFD predicted**

Fig. 4 Time histories of dynamic fluid forces for various diffuser vanes' number (N = 1750min^{-1}, ϕ/ϕ_0 =1.0)

Figure 4 indicates the time histories of the measured and calculated unsteady hydrodynamic forces during two revolutions of the test impeller. The experimental data are phase-averaged for 55 revolutions of the impeller, while the results calculated by CFD are not phase-averaged but instantaneous. The waveform of unsteady hydrodynamic forces calculated by CFD shows good agreement with the experimental data. The lack of higher frequency in the pressure predicted by RANS code shows that RANS method has some limitation in unsteady flow applications.

As shown in Fig. 4, the unsteady hydrodynamic forces for $Z_d = 6$ are much smaller than those for $Z_d = 5$, and show the trends similar to that for $Z_d = 0$ without interaction between the impeller and diffuser vanes. The small hydrodynamic forces for $Z_d = 6$ are due to the circumferentially symmetric arrangement of the vanes. The fluid forces are the results of the integration of the pressures due to the interaction between the impeller blades and the diffuser vanes. The interaction occurs simultaneously between each impeller blade and diffuser vane for $Z_d = 6$. The same amplitude of the pressure fluctuations results in smaller amplitude of fluid forces for $Z_d = 6$.

Unsteady Pressure in Vaned Diffuser Passage

Figure 5(a) indicates the time history of unsteady part of the instantaneous pressure coefficient on the suction side pressure tap (r_1, c_1) near the diffuser vane leading edge[4]. The waveforms of unsteady pressure calculated by CFD and the vortex method show good agreements with the measured one. The magnitude of the pressure fluctuations predicted by vortex method, however, is the biggest because of the 2-D flow assumption in the calculation. The power spectral density function shown in Fig. 5(b) demonstrates that the pressure fluctuates with the impeller blade passing frequency NZ_i and its higher harmonics. A good agreement can be seen between the measured frequency components and those calculated by the vortex method and CFD.

Figure 6 shows the comparisons of the pressure fluctuations for Z_d=6 and Z_d=5 on the pressure taps (r_1, c_1) and (r_3, c_1) predicted by CFD. As shown in Fig. 6, the fluctuations of the unsteady pressure decay much more slowly for $Z_d = 6$ than that for $Z_d = 5$ with the increasing radius. Comparing the magnitudes of the unsteady pressure, it can be found that the magnitude of the pressure fluctuations for $Z_d = 6$ is much bigger than that for $Z_d = 5$. And higher frequency components are larger for $Z_d = 6$ than those for $Z_d = 5$. The local pressure fluctuation is larger when the vanes number on the impeller and diffuser is identical, and should not be neglected in actual engineering design. The interaction between every impeller blade and diffuser vane occurs simultaneously for the diffuser with 6 blades. The pressure fluctuations have the same amplitude and phase in this case,

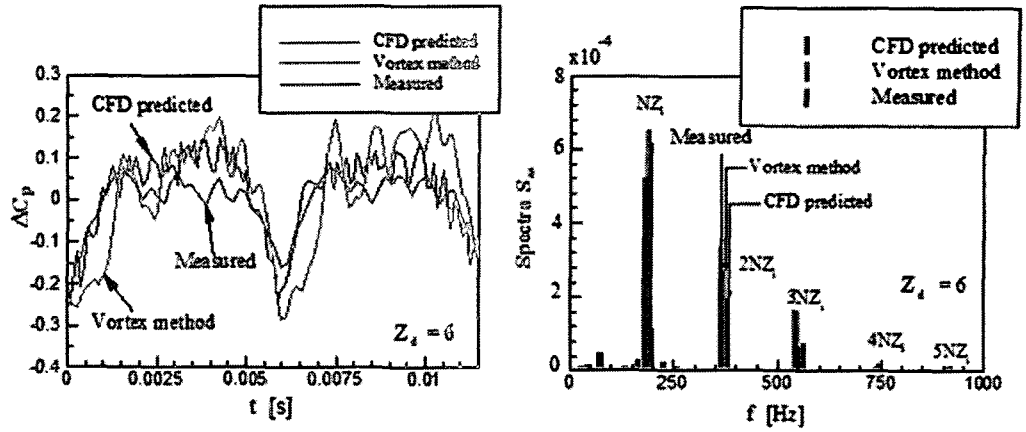

(a) Time histories of ΔC_p (b) Power Spectrum

Fig. 5 Pressure fluctuation at station (r_1, c_1); ϕ/ϕ_0=1.0

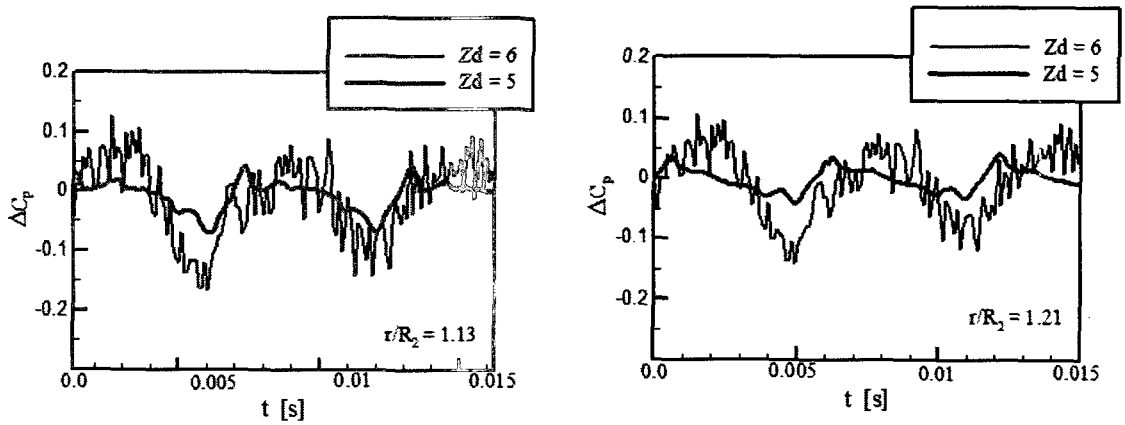

(a) Station (r_1,c_1) (b) Station (r_3,c_1)

Fig. 6 Calculated pressure fluctuation in vaned diffuser passage; ϕ/ϕ_0=1.0

and thus the circumferential pressure gradient is stronger than for non-identical number of impeller and diffuser vanes. Therefore, the diffusion of pressure may be weaker in downstream direction because of stronger circumferential pressure gradient.

Figures 7 (a) and (b) show the CFD predicted and measured instantaneous pressure at pump inlet for Z_d = 6 and Z_d = 5. The effect of the length of the suction pipe is also calculated using two different pipe lengths, 150mm and 250mm. The pressure fluctuations for Z_d = 6 are found to be much larger than that for Z_d = 5. The suction pipe length has little effect on the pressure fluctuation at pump inlet. As can be seen in this figure, the unsteady pressure has much larger magnitude for Z_d = 6 than that for Z_d=5.

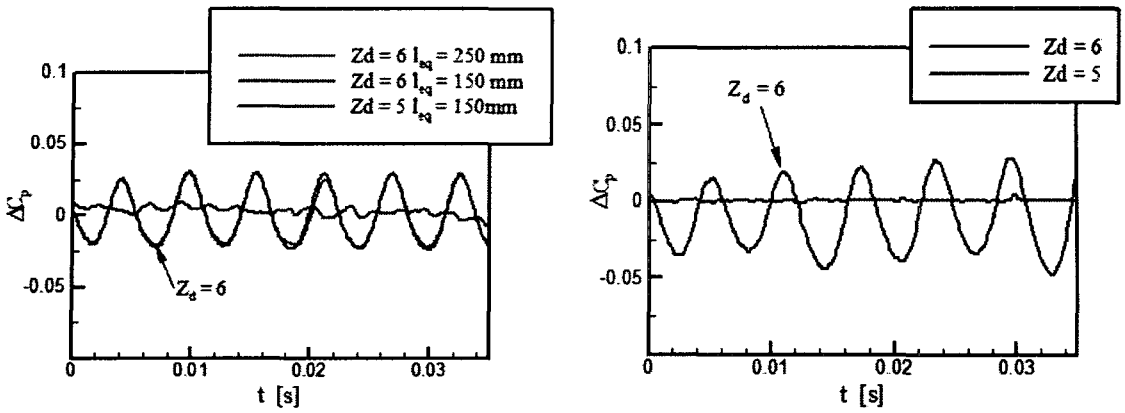

(a) CFD predicted **(b) Measured**

Fig. 7 Pressure fluctuations at pump inlet; $\phi/\phi_0 \doteq 1.0$

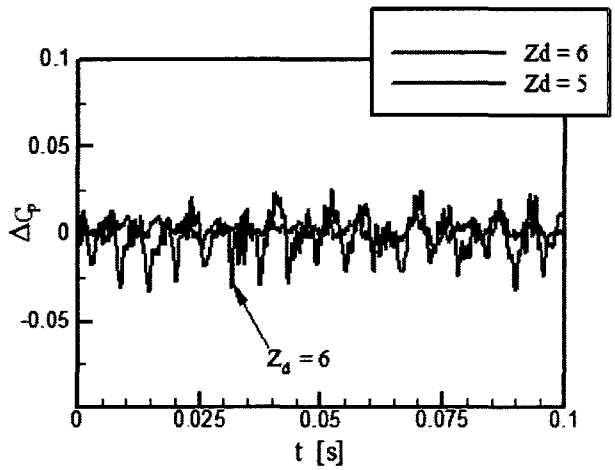

Fig. 8 Calculated pressure fluctuation at pump discharge

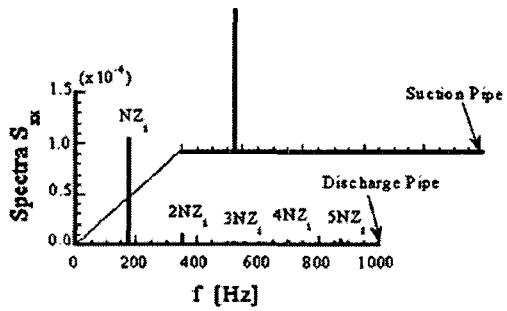

Fig. 9 Power spectra of measured pressure fluctuation at pump suction and discharge

Figure 8 shows the CFD predicted pressure fluctuation in the pump discharge. As shown in this figure, the pressure fluctuation has a larger magnitude for $Z_d = 6$ than for $Z_d = 5$, and the pressure fluctuations in the pump discharge have almost the same magnitude as that in the pump inlet.

Figure 9 shows the power spectrum density of the measured unsteady pressure at the pump inlet and discharge. As shown in this figure, the dominant frequency of the unsteady pressure at the pump inlet is NZi, while the higher harmonies are also dominant at the pump discharge in addition to the NZi component. The unsteady fluctuations are very weak for the other combinations of the number of impeller and diffuser vanes. So it can be concluded that the larger fluctuation of the inlet and discharge unsteady pressures is not due to the resonance of the pipe system, but is caused

by the strong potential interaction which decays more slowly.

Conclusions

As the result of the experimental and numerical studies of the rotor-stator interaction in diffuser pumps, the following conclusions have been derived:

(1) Sources contributing to the pressure fluctuations in the diffuser passage of the diffuser pump stage have been captured with a 2-D RANS solver as well as vortex method: potential interactions cause the highest peak of pressure in the diffuser; viscous wakes shed from the impeller interfere with the successive diffuser vanes and result in the presence of additional high pressure peaks.

(2) The frequency components of the pressure fluctuations in the diffuser passage are comprised mainly of the impeller blade passing frequency Z_iN and its higher harmonics of $2Z_iN$ and $3Z_iN$. This indicates that the impeller-diffuser interaction is caused chiefly by potential interaction and wake impingement with the diffuser vanes.

(3) The "jet-wake" flow structure at impeller discharge affects the wake-diffuser interaction, but it is relatively small compared with stronger viscous wake interactions in the present pump.

(4) There exist some lower dominant frequencies in the pressures downstream of the impeller for unstable range because of the effects of the complicated flows such as separating flow, rotating stall and reverse flow in pumps. These lower dominant frequencies are dependent on the flow rate and the unsteady pressures are chaotic in these unstable ranges.

(5) The unsteady flow may be classified into several ranges based on the flow structures.

(6) The combination of impeller and diffuser with identical vane numbers can be employed because of its smaller unsteady forces, although the pressure fluctuations are bigger compared with other combination cases:

   (i) The hydrodynamic forces acting on the diffuser pump impeller are smaller when the number of vanes on the rotor and stator is identical because of the circumferentially symmetrical arrangement of vanes.

   (ii) The local pressure fluctuations in the diffuser passages downstream of the impeller have larger magnitude when the number of the impeller vanes equals to that of the diffuser. And the decay of the pressure fluctuations downstream is slow. Moreover, the pressure includes the higher harmonics of blade passing frequency.

Nomenclature

b_2 = impeller discharge width

C_p . . . . . = pressure coefficient, $(p + \rho gh - P_s)/(u_2^2/2)$

CS = control surface

c = symbol of pressure traverse line

F_x, F_y = hydrodynamic force in x and y direction

f = frequency

H = total head

h = height

K_x, K_y = normalized hydrodyanmic force components, $K_{x,y} = F_{x,y}/(\rho u_2^2 \pi D_2 b_2 / 2)$

N = rotational speed

PS = pressure side

P_s = total pressure at suction port

p = static pressure

r, θ, z = radial, tangential, and axial direction, respectively

SS = suction side

S_{xx} = Power spectrum density

t = time

u_2 = peripheral speed of impeller [m/s]

X, Y = stationary coordinates

Z = number of vanes

ϕ = flow coefficient

ρ = density

σ = standard deviation

ψ = total head rise coefficient

ψ_{imp} = impeller characteristic, $2g(H_{CSII}-H_{s2})/u_2^2$

$\Delta\psi_d$ = hydraulic loss in the guide vane, $2g(H_{CSII}-H_{d1})/u_2$

ΔC_p = nondimensional unsteady pressure $= C_p - \overline{C_p}$

Subscripts

d = discharge side; diffuser

i = impeller

s = suction side

r, 0 = rated

X, Y = component in X and Y direction

Superscript

- = time averaged

References

[1] Wang, H., and Tsukamoto, H., 2003, "Experimental and Numerical Study of Unsteady Flow in a Diffuser Pump at Off-Design Conditions", ASME Journal of Fluids Engineering, Vol.125, pp.767-778.

[2] Funakoshi, H., Tsukamoto, H., Miyazaki, K., and Miyagawa, K., 2003, "Experimental study on unstable characteristics of mixed-flow pump at low flow-rates," ASME 2003 Fluids Engineering Division Summer Meeting, FEDSM2003-45103.

[3] Sano, T., Yoshida, Y., Tsujimoto, Y., T., Nakamura, Y., and Matsushima, T., 2002, "Numerical Study of Rotating Stall in a Pump Vaned Diffuser," ASME Journal of Fluids Engineering, Vol.124, pp.363-370.

[4] Zhang, M., Wang, H. and Tsukamoto, H., 2002, "Numerical Analysis of Unsteady Hydrodynamic Forces on a Diffuser Pump Impeller Due to Rotor-Stator Interaction," Proc. of FEDSM 02, Montreal, FEDSM2002-31181.

[5] Zhang, M., and Tsukamoto, H., 2005, "Unsteady Hydrodynamic Forces Due to Rotor-Stator Interaction on a Diffuser Pump With Identical Number of Vanes on the Impeller and Diffuser," ASME, Journal of Fluids Engineering, Vol. 127, No. 4, pp. 743-751.